This paper describes objective technical results and analysis. Any subjective views or opinions that might be expressed in the paper do not necessarily represent the views of the U.S. Department of Energy or the United States Government.

SAND2019-3986J

**Article Type: Materials science**

**Corresponding Author:** Dick C. Engbrecht, 738 S Patton Circle, Arlington Heights, IL 60005, USA
Email: dce_caso4@comcast.net

# Title: Measurement of Heat Flow through Cast Slabs of Calcium Sulfate Dihydrate

## Authors:

Dick C. Engbrecht, 738 S Patton Circle, Arlington Heights, IL 60005

Deidre A Hirschfeld, Manager, Coatings & Additive Manufacturing Dept., Sandia National Laboratories, PO Box 5800, MS 0959, Albuquerque, NM 87185-0959



Sandia National Laboratories is a multimission laboratory managed and operated by National Technology & Engineering Solutions of Sandia, LLC, a wholly owned subsidiary of Honeywell International Inc., for the U.S. Department of Energy's National Nuclear Security Administration under contract DE-NA0003525.

**Abstract:** Slabs of cast calcium sulfate dihydrate have been used for decades as a heat transfer barrier in commercial and residential construction and are assessed in accordance with the parameters defined by ASTM C1396. The study described herein hypothesizes that minor impurities have significant effects on the high temperature performance of these casts. Five thermocouples are cast into a 20 mm thick slab at about 4 mm intervals are measured between ambient and ~1000°C in a furnace. Thermal diffusivity and inertia are estimated from this temperature profile. This study compares natural, flue gas desulfurized (FGD) and reagent grade hemihydrates that have been converted into the dihydrate form with distilled water; the common additives kaolin and borax are used to modify the cast. The thermocouple data allow an effective thermal diffusivity (α') and an effective thermal inertia (I') to be calculated. The hemihydrate source and kaolin content are found to affect the high temperature performance; the FGD source increases the thermal inertia, Kaolin inhibits the formation of other borate compounds through intercalation.

Keywords: gypsum, hemihydrate, kaolin, borax, thermal diffusivity, thermal inertia

## 1. Introduction

The calcium sulfate system has three possible phases; dihydrate ($CaSO_4 \cdot 2H_2O$) which is stable <~80°C, hemihydrate ($CaSO_4 \cdot ½H_2O$) which is metastable and forms ~150°C and can be recrystallized to the dihydrate when mixed with water, and anhydrite ($CaSO_4$) which is stable and forms at >225°C. These phases also exist as minerals but this paper is restricted to these phases as they are used and exist in manufactured products. In a high temperature situation, such as a fire, the metastable phase is simply included in the total mass loss because heat is continuously applied and the dehydroxylation proceeds directly to anhydrite.

Since the introduction of gypsum (calcium sulfate dihydrate) panels into commercial and residential construction in the early twentieth century, various additives have been incorporated into these panels to extend the barrier properties under fire (high temperature) conditions with particular emphasis placed on dimensional stability[1]. The patent literature is replete with various additives that fall into the general categories of glass fibers, various clays, vermiculite, perlite, fly ash, and many others. Other anecdotal evidence describes enhanced high temperature protection from additives such as those used to impart resistance to water in the liquid and vapor phases (siloxane and sodium trimetaphosphate, respectively). When these panels are tested for performance when exposed to fire as prescribed by ASTM C1696 [2] and ASTM E119 [3] producers of these panels obtain different results even when made from the same formulation at different manufacturing sites without thoroughly understanding why.

The manufacturing process introduces compositional changes when the hemihydrate is fluidized with water primarily through the dissolution and recrystallization process when ions from impurities and additives are included in the crystalline matrix. Additional compositional changes happen during the drying process when hot water and steam soluble impurities and additives are dissolved and deposited at the evaporation plane. The product is relatively stable, but can be affected by humidity when it contains deliquescing salts, until it is exposed to temperatures that exceed the calcination point of gypsum [3-6].

The fire modeling community that studies the transient thermal conduction nature of the gypsum wallboard passive barrier [7] generally discounts that the slab provides any beneficial properties, other than as an intact thermal barrier, once the crystalline water has been evaporated with the conversion from the dihydrate to anhydrite calcium sulfate phases, which occurs at ~250°C. [8, 9] Later studies, discussed below, recognized the importance of other compounds,

such as clay, borax and other hydrated minerals, and components, such as glass fibers and vermiculite, which were being added into commercial products. Researchers evaluated these factors for their effects at temperatures >250°C hypothesizing that endotherms at this elevated temperature will affect the performance of wallboards.

Several researchers have investigated some of the additives. Baux *etal* [10] studied the effects of silica fume and reported that benefits included blocking the formation of microcracks and increasing the compressive strength as the density decreases but adversely affected the thermal conductivity and latent heat.

Ciudad *etal* [11] investigated three alkaline earths (MgOH, CaOH, and $CaCO_3$) as potential additives because they have endothermic responses in the same temperature range and should provide additional protection beyond that of just gypsum. These three additives distributed four endothermic zones along the temperature profile between ambient and 1000°C demonstrating improved performance over gypsum alone.

Waclawska [12] described reactions and thermal changes in borax and related compounds that could occur during the fluidization phase in the use of the hemihydrate. One of the compounds, Ulexite ($2CaO \cdot Na_2O \cdot 5B_2O_3 \cdot 16H_2O$) , is synthesized by the chemical reaction between the $CaSO_4$ and borax; the effect of Gerstley borate on castings was also noted to affect the shrinkage [13].

A mechanism explaining the beneficial effect of kaolin is discussed by Sugahara [14] by describing the intercalation process in which ions are incorporated into the kaolin crystal in the water layer between the silicate sheets. This mechanism explains the changes in the performance when kaolin was added to mixtures, which has ion exchange properties that prevent the formation of the lower melting point borate compounds.

Sedighi-Gilani *etal* [15] studied the release of moisture in gypsum board up to 600°C and reported that the water accumulated in the gypsum core-paper interface but recommended that future studies investigate the compositional effects incurred by the movement of water through the board to the evaporation plane.

Shepel *etal* [16] also studied vapor transport and its effect on heat transfer and reported that it was affected by the permeability of the core and the paper liner. It was concluded that the amount of condensate was low and could be neglected in models on fire behavior.

Keerthan *etal* [17] investigated the parameters reported by several modelers and concluded that new parameters were needed primarily to address ablation and an endotherm at a higher temperature, ~800°C, than those in existing models. A new set of equations describing thermal conductivity and the specific heat were developed from empirical data and used to validate the model presented when $CaCO_3$ is present in gypsum board.

A common theme in these studies is that the effect of additives is not well understood. The validation data for the models is primarily based on full scale ASTM E119 [3] studies using paper-covered gypsum board. In a full scale test, thermocouples are placed on the surfaces of the panels and between the panels and studs on which the panels are mounted. In a study by Wullschleger *etal* [18] an effort is made to monitor internal core temperatures by milling slots at depths of 4 mm and 8 mm in a 12 mm thick panel. The slots containing the internally mounted thermocouples are filled with a gypsum setting compound to protect and fix the thermocouples in place. The surface mounted thermocouples are mounted using sodium silicate to affix the thermocouples to the internal and external surfaces. The specially prepared panels with the thermocouples in place were placed in the furnace used to run an International Standard Organization ISO 834-1 fire resistance test and exposed to ~1000°C for 45 minutes. Evaluation

of panels for thermal conductivity at 20°C ($\lambda$, $W \cdot m^{-1} \cdot K^{-1}$) gave values of 0.28 ± 0.02 for panels as received, 0.14 ± 0.01 for panels calcined at 200°C for 2 days, and 0.27 ± 0.02 for panels exposed in the furnace at 1000°C for 45 minutes, which could be concluded to mean that once all of the components had completed their thermal responses then maintaining the physical integrity of the panel was a critical performance factor. These data are used to validate the model generated in the Wullschleger paper, which showed that varying the gypsum dehydration enthalpy and specific heat significantly affected the room side temperature that defines success and failure in the fire resistance test.

The study described herein provides qualitative information on the movement of heat through a slab consisting of different hemihydrate sources and two common additives. No paper or glass mat coverings were used that could interfere with the heat flow into specimens. There was no intention to provide a model of a fire test but to consider the properties of the barrier material known colloquially as gypsum wallboard solely rather than as a part of system as defined by ASTM C1396, C1278 and C1178 within the context of an ASTM E119 test. The intent was to provide material data that can be used like any other component; for example, like wood properties such as moisture content, density, char rate, *etc* are often used as inputs to fire models. Furthermore in construction, each system, which consists of barrier and support materials, must be certified to a specific time rating.

## 2. Experimental

Gypsum slabs were prepared with cast-in-place thermocouples from three different hemihydrates, which were selected from a natural source, a flue gas desulfurized gypsum (FGD) source, and a reagent grade source [19]. Kaolin and borax were added to each of the hemihydrates using a designed experiment to facilitate analysis. These two minerals were listed in the patent literature as typical additives in gypsum boards designed for high temperature exposure. Each slab was heated in a custom designed furnace equipped with quartz windows so that changes to the surfaces on the furnace side and ambient sides could be observed and documented with a digital camera [20].

### 2.1 Casting Mold

A silicone rubber mold, shown in Figure 1, for making the slabs (150 mm x 150 mm x 20 mm) was prepared with random surface imperfections and an indentation for placing an alumina thermocouple array in the cast. The random surface imperfections were created by sprinkling MgO powder randomly onto the surface of a high-density polyethylene (HDPE) form and binding them together with lacquer. An indentation to accept the thermocouple array (10 mm x 5 mm x 2 mm) was created in the base of the mold so that the array is placed in approximately the same location of each cast. The holder was placed ~50 mm from the edge of the HDPE form and centered along the length of the HDPE form. A frame surrounded the HPDE form and had a slot that aligned with the thermocouple holder to allow thermocouples to exit from the casting. The entire mold was approximately 200 mm x 200 mm x 75 mm and filled with a catalyzed, high strength silicone rubber. The form was removed from the silicone rubber casting and cleaned of all flash and foreign materials.

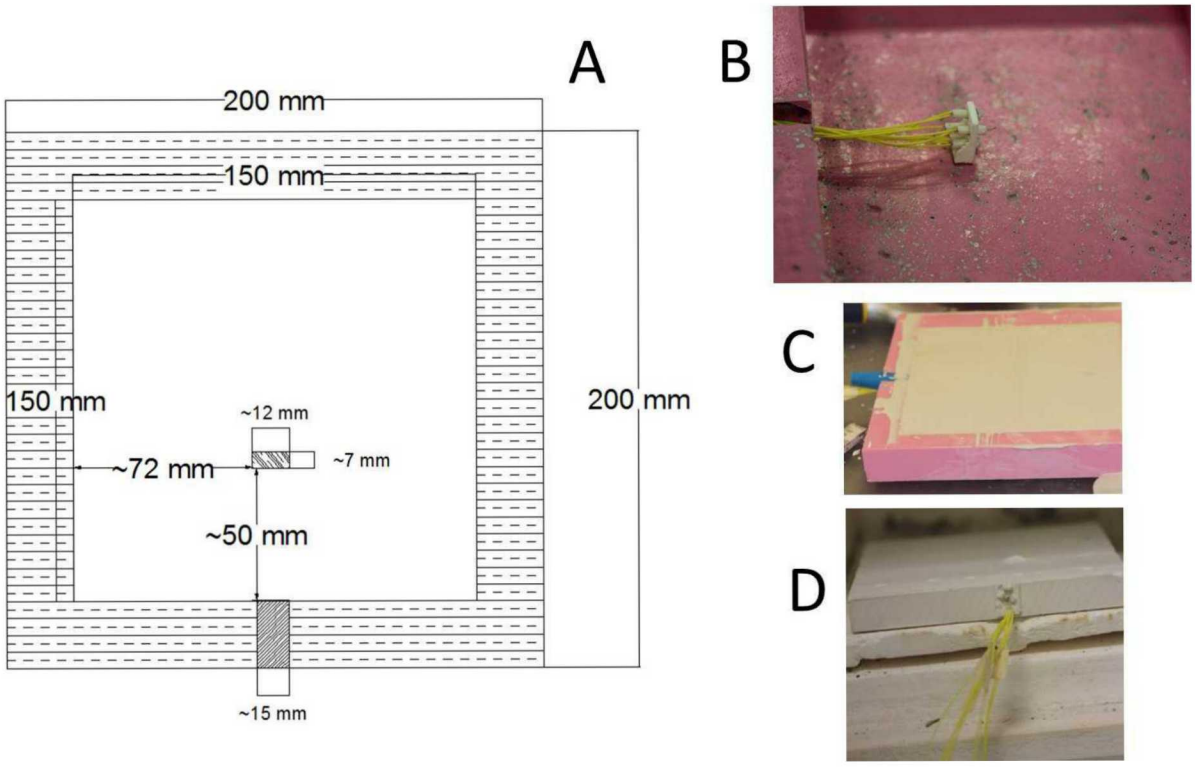


Figure 1: Silicone Mold for Casting Slabs; A – sketch of mold showing dimensions, B – finished mold with thermocouple placement, C – filled mold, and D – side view of mold showing thermocouple wires exiting mold.

## 2.2 Thermocouple Array

A high temperature resistant array was designed to be cast into the slab such that the thermocouples would always be placed the same distance from the outer surfaces of the cast. The array had to be resistant up 1100°C and able to accept fine thermocouple wires (0.005 in [0.125 mm], bare wire, Type K) that were threaded through a 2-hole alumina rod to keep the wires separate. The wires were covered with Teflon™ insulation. Each completed array was weighed to ensure accurate mass measurements of the slabs to calculate the density. The array dimensions are shown in Figure 2.

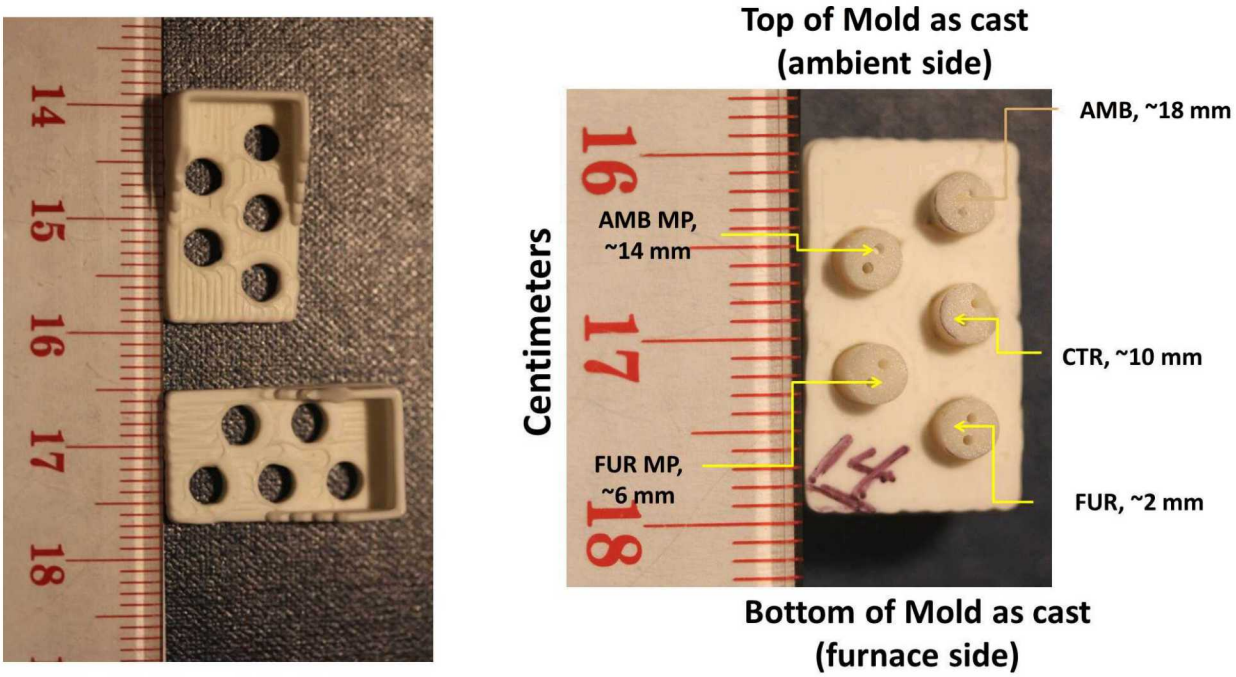


Figure 2: Alumina thermocouple array holder; custom design made by www.robocasting.com

## 2.3 Experimental Design

The design used the general linear model (GLM) with 2-levels of factor one (kaolin – 0 or 5%, 2-levels of factor two (borax – 0 or 0.4%), and 3-levels of factor three (hemihydrate source – natural, FGD, or reagent) based on the hemihydrate mass (450 g). This design permitted the analysis of the main factors only, or analysis of the experiments in subset of $2^3$ full factorials; kaolin:borax:natural-FGD, kaolin:borax:natural-reagent, and kaolin:borax:FGD-reagent. Two sources of commercially prepared hemihydrate [19] were selected to be representative of the two categories of commercially available sources (natural source and FGD source) and a reagent grade source. Distilled water (675 mL) was used to fluidize the mixture.

## 2.4 Slab Preparation

Prior to use, the temperature readings from each thermocouple array were recorded while placed in an ice bath, hot water bath, and in the ambient lab conditions to determine discrepancies among them and insure that all were functioning properly; the thermocouples were recorded throughout the hydration phase until removal from the mold.

The mold was lightly coated with WD-40® to facilitate specimen removal. A prepared thermocouple array was located into the mold and the exit slot for the wires was sealed with modeling clay. The selected hemihydrate source was dry blended with kaolin, borax, or both. The blend was added to distilled water (150% of hemihydrate mass) and allowed to soak for 60 seconds, and mixed in a blender on low speed for 25 seconds. The slurry was poured immediately into the prepared silicone mold, smoothed and allowed to hydrate for about 45 minutes. The specimens were removed from the mold, cleaned of flashing, measured, weighed and placed in a drying cabinet at 40°C until the weight did not vary by more than 0.01 grams in 2

hours. The specimens were cooled to ambient temperature and stored in a sealed plastic bag until testing.

**2.4 Furnace –**

A VCella model 11 kiln (Chula Vista, CA) was modified with a custom door to accept the prepared slabs as shown in the left panel of Figure 3. A programmable controller was used to control the heating profile. The ramp rate, shown in the right panel of Figure 3, was varied because the furnace could not keep up at the higher temperatures due to the quartz viewing ports in the front and back furnace walls.

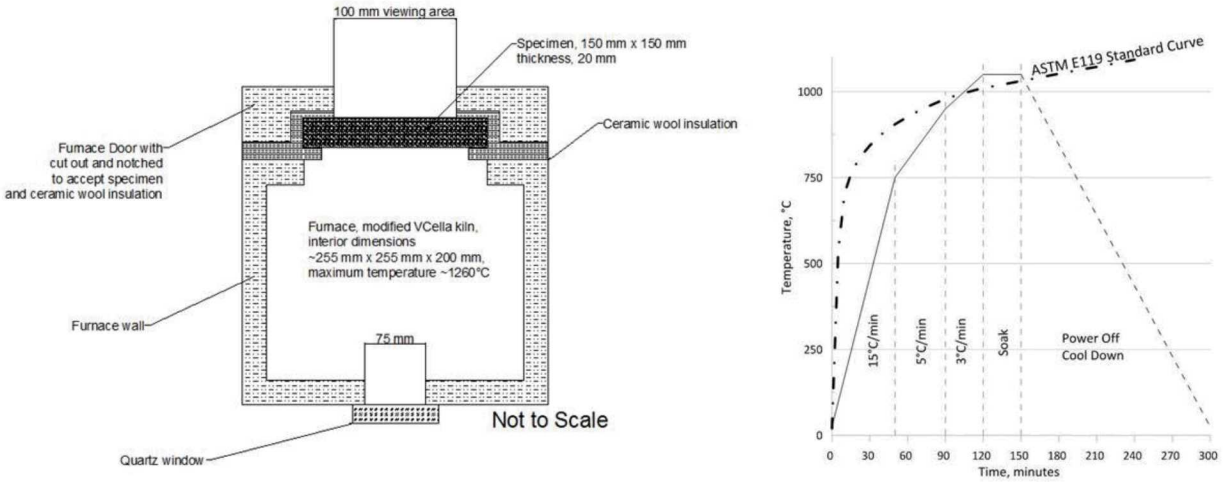


Figure 3: Furnace used to test slabs (left) and the actual heating profile compared to the ASTM E119 standard curve (right).

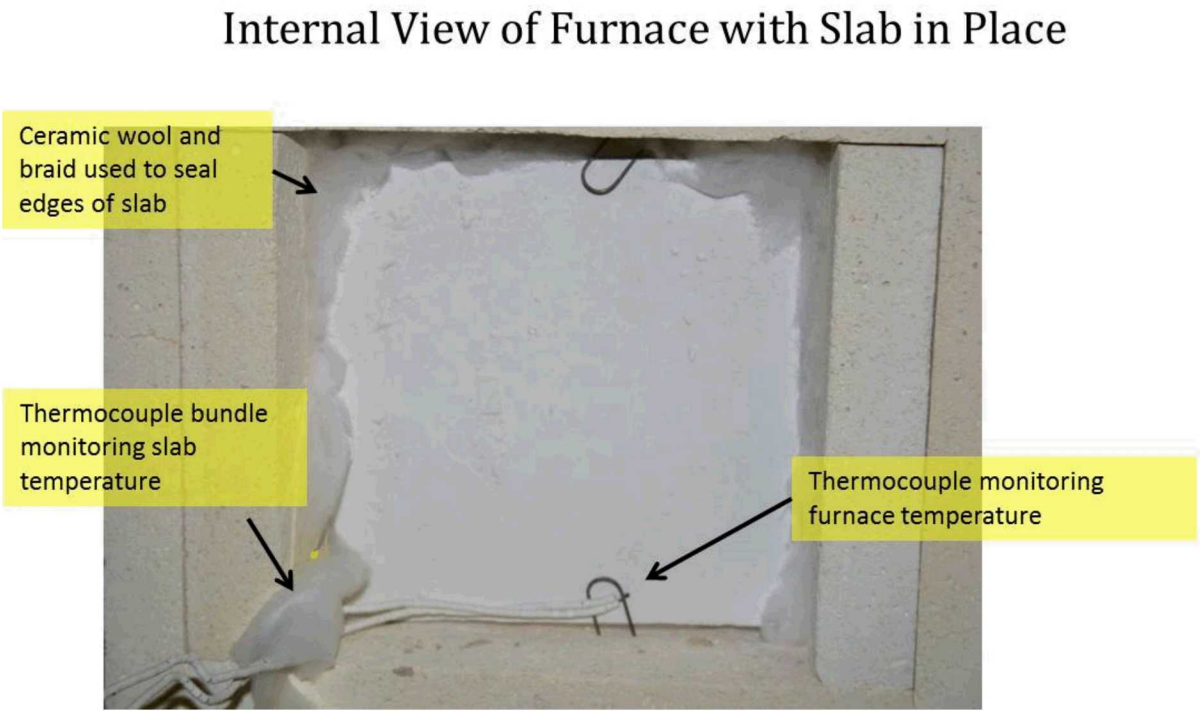

Figure 4: Slab mounted in furnace prior to heating.

## 2.5 Furnace Data Collection

The thermocouples in the slab were connected to the data acquisition device before testing was started to insure that all of them were still functioning. Two additional thermocouples (Type K, AWG 20, "fish scale" ceramic insulation) were placed; one on the ambient side of the slab adjacent to a ¼" quartz plate that covered the specimen and a second one was placed approximately 2 mm away from the furnace side of the slab. The data from the five embedded and two external thermocouples were obtained every 5 seconds for the duration of the test. Figure 4 depicts the arrangement of the specimen during the test.

## 2.6 Interpretation of thermocouple data; effective thermal diffusivity (α') and effective thermal inertia (*I'*)

The qualitative linear approach is used as an estimation of the many kinetic and thermodynamic changes that occur in the structure of the gypsum based casts during the forming, drying and heating stages in the use of gypsum as a thermal barrier.

The data from each heating cycle display a pattern common to all gypsum dehydrations (Figure 5), *i.e.*, an induction period, followed by a steady temperature period, designated as Calcination, where the crystalline water is evaporated. A second intermediate period, designated as Mid-Range, where the anhydrite crystal is reordered from monoclinic to orthorhombic and other changes may occur such as a kaolin endotherm and a borax exotherm. A third period marked by a sharp change in slope, designated as Hi-Range where heat is being transferred through the barrier of anhydrite and other constituents found in or added to the original casting formulation. To facilitate the interpretation of these data, the approach used by Wickstrom [7] is adapted to provide a qualitative assessment of the "thermal diffusivity and thermal inertia" in the

boundary condition (BC) called "Constant Surface Temperature: First Kind of BC" and "thermal inertia" in the boundary condition called "Constant Gas Temperature: Third Kind of BC". The terms "*effective thermal diffusivity"* and *"effective thermal inertia"* are introduced and utilized as a qualitative approach to characterize a very complex interaction of process and structure. This is not meant as a technique for evaluating real structures but rather a technique to compare the effects of the materials by consolidating the dynamic changes into a value that reveals the thermal and compositional changes observed in this experiment.

Gypsum castings are a complex mixture of a sulfate salt, which is predominantly $CaSO_4 \cdot 2H_2O$, and smaller amounts of a foaming agent, an organic dispersant, starch, polyvinyl alcohol or polyvinyl acetate, organic and inorganic fibers, chlorides, clay, silica and silicates, carbonates, and any number of other compounds being carried in the flue gas stream. All of these components are further confounded when mixed with water (20°C-40°C) and the hemihydrate phase which will form any number of other compounds and additional reactions in hot water (~75°C) during the drying stage of the manufacturing process. This being said, the system is too complex to estimate values for *thermal conductivity* at each slope change in the ranges highlighted in Figure 5. Thermal diffusivity is defined as conductivity divided by heat capacitance or heat flux penetration speed –

$$\alpha = \frac{k}{\rho c_p},$$

where k = heat conduction ($W \cdot m^{-1} \cdot K^{-1}$), $\rho c_p$ = heat capacity per unit volume ($J \cdot m^3 \cdot K^{-1}$), and thermal inertia as the square root of the conductivity multiplied by heat capacitance or the speed of temperature increase [7, 21]. This relationship can also be expressed as

$$\frac{\partial^2 T}{\partial x^2} = \frac{1}{\alpha\prime}\frac{\partial T}{\partial t}$$ and rearranged to $\alpha' = \frac{\partial T/\partial t}{\partial^2 T/\partial x^2}$

An estimation of an *effective* thermal diffusivity (α', $m^2 \cdot s^{-1}$) and an *effective* thermal effusivity (*effective thermal* inertia, I', $J \cdot m^{-2} \cdot K \cdot s^{-½}$) can be made using the plot of time vs temperature. The data for the CTR thermocouple were used to determine the regression equation in each period for the *effective thermal diffusivity*; see example in Figure 5. The data from each thermocouple were selected at a specific time, *e.g.*, 8000 seconds in the Hi-Range, and a second order regression was conducted on the temperature at that specific time for each thermocouple between 2 mm and 18 mm for *effective thermal inertia.*

The relationship between the temperature and time ($\delta T/\delta t = k$) is a simple linear regression equation, which has the general form:

$$y = c + \alpha X .$$

The slope of the line in the sections identified in Figure 5 is used as the estimate for k.

The volumetric heat capacity ($\rho c_p$, $J/m^3 \cdot K$) is a measure of the amount of heat stored in the material [22]. In this study, the curvature of the distance:temperature relationship in the section shown in Figure 5 is used as an estimate for $\rho c_p$. The relationship of the temperature and thermocouple depth ($\delta^2 T/\delta x^2 = \rho c_p$) is a second order equation, which has the general form:

$$y = c + bX + aX^2 .$$

This term is obtained from the second derivative of the regression equation, which equals 2 times the coefficient of the squared term (2a). The absolute value of the second order term is used in all calculations, when the coefficient is negative

The calcination phase obtained on the reagent source with 'no additives' is used in an example of the determination of the *effective thermal diffusivity* (Figure 6A) and *effective thermal inertia* (Figure 6B).

The *effective thermal diffusivity* (α') is determined –

$$\alpha' = \frac{\partial T/\partial t}{\partial^2 T/\partial x^2}.$$

$$\alpha' = \frac{0.056}{|2x0.0088|} = \frac{0.056}{0.0176} = 3.181 \text{ mm}^2 \cdot \text{s}^{-1}$$

and when converted to standard units of $m^2/s$ ...

$$\alpha' = \frac{3.181}{10^6} = 3.181 \times 10^{-6} \text{m}^2 \cdot \text{s}^{-1}$$

; typical diffusivity values [22] ($m^2 \cdot s^{-1}$) for some common building materials similar to gypsum are – marble $1.2x10^{-6}$, concrete $0.75x10^{-6}$, brick $0.52x10^{-6}$.

The *effective thermal inertia* (I') is determined –

$$I' = \sqrt{\delta T/\delta t \times \delta^2 T/\delta x^2}$$

$$I' = \sqrt{0.056 \times |2 \times 0.0088|} = \sqrt{0.0009856} = 3.1394 \times 10^{-2} \text{ J/mm}^2 \cdot \text{K} \cdot \text{s}^{1/2}$$

and when converted to standard units of $J/m^2 \cdot K \cdot s^{1/2}$ …

$$I' = \frac{3.1394 \times 10^{-2}}{10^6} = 3.139 \times 10^{-8} \text{ J/m}^2 \cdot \text{K} \cdot \text{s}^{1/2}$$

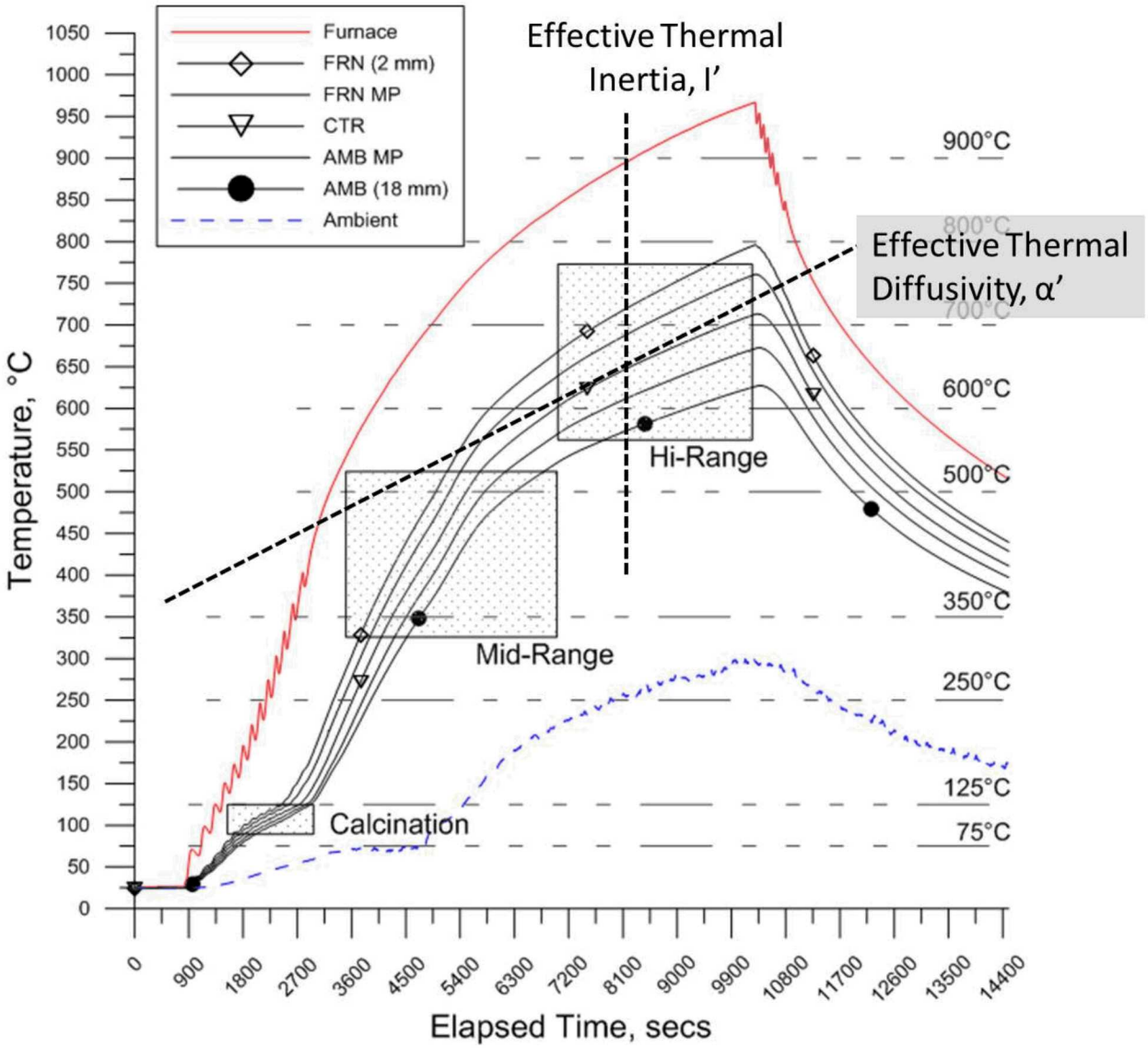


Figure 5: Typical temperature profile of gypsum slab during the furnace heating profile and nominal distance from the furnace side of the slab; FRN - ~2 mm, FRN MP - ~6 mm, CTR - ~10 mm, AMB MP - ~14 mm, and AMB - ~18 mm; Effective thermal diffusivity, α' shows where linear regression was obtained for Hi-Range values; Effective thermal inertia, I' shows where quadratic regression was obtained for Hi-Range values at a constant time. Similar areas were analyzed on the CTR trace for the Calcination and Mid-Range regressions.

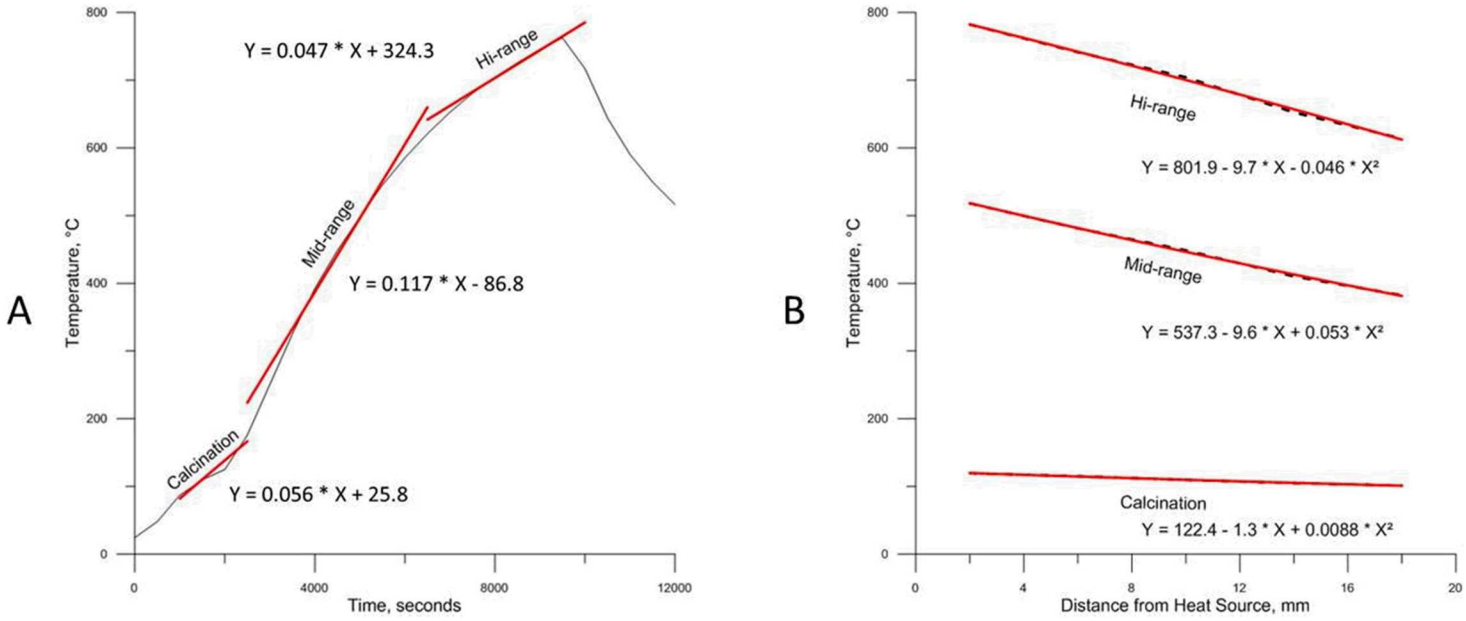


Figure 6: Example showing calculations for (A) effective thermal diffusivity, k and (B) effective thermal inertia, $\rho c_p$.

## 3. Results and Discussion

The tests were conducted in random order to limit the effect of any bias in the testing cycle. The specimens were weighed and the thermocouples were tested after inserting in the furnace but before the power was turned on to insure all were functioning properly.

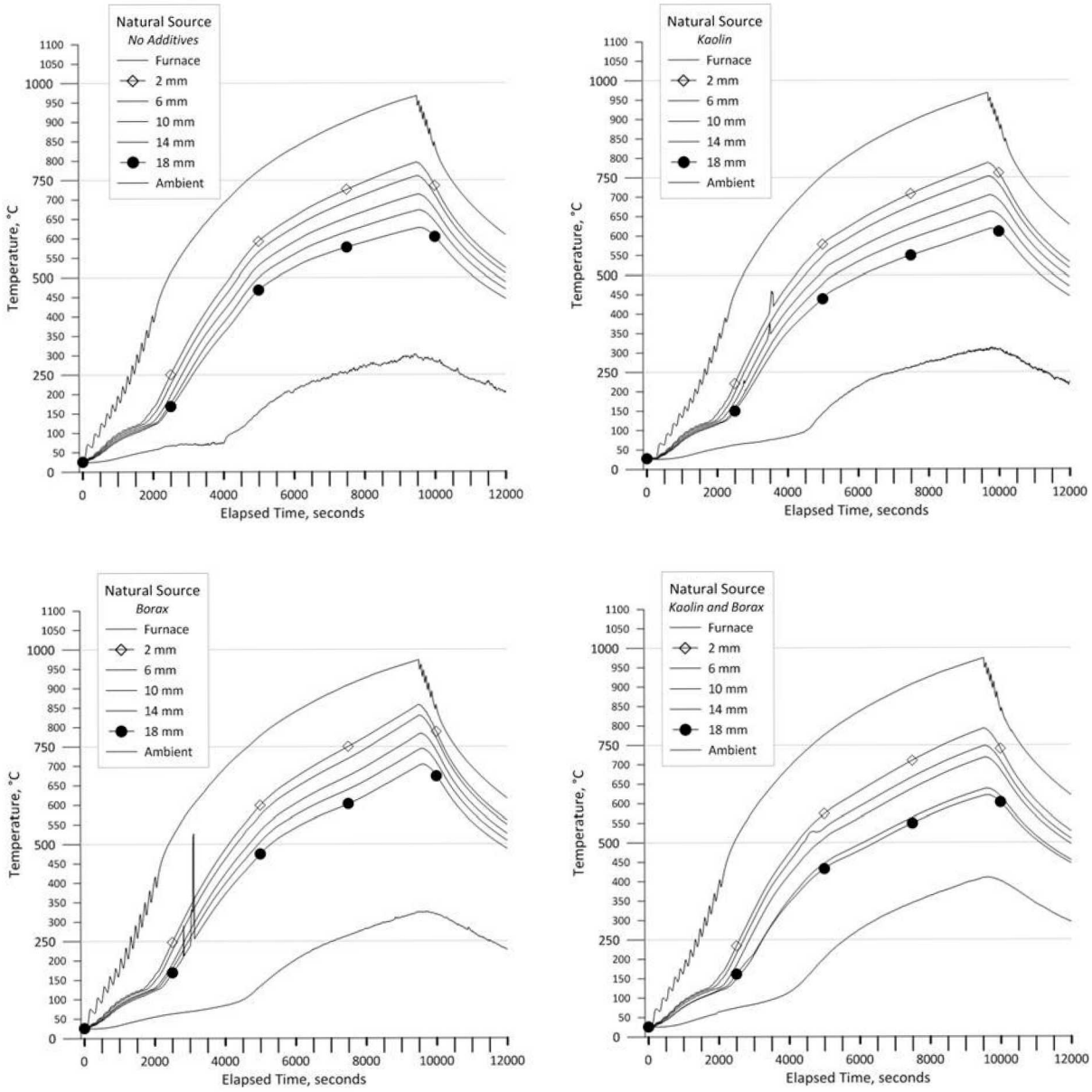


Figure 7: Natural Source - Embedded thermocouple temperatures; legend shows order of thermocouples from furnace side to ambient side.

The results of the embedded thermocouple data are graphically summarized in Figure 7, Figure 8, and Figure 9 by source; natural, FGD and reagent, respectively. The data determined for the effective thermal diffusivity and effective thermal inertia are shown in Table 1, **Error! Reference source not found.**, and Table 3 by source; natural, FGD, and reagent, respectively.

Several of the traces show a temperature spike on one or more thermocouples. The spikes were considered anomalies in the data and were removed by interpolation between the end points of the steady trace; unless the spikes were replicated as the heat transferred through the slab which did not occur in this study. The FGD borax plot (lower left, Figure 8) had a data acquisition failure on the furnace thermocouple; the furnace trace in this plot is the average of ten of the traces. The reagent borax plot (lower left, Figure 9) encountered thermocouple failures on the 2-mm and 6-mm thermocouples and a complete failure on the 10-mm thermocouple near the maximum temperature; this test also incurred a power failure at about the 5200 second mark indicated by the "flat" section in the trace. The history of the traces on the other thermocouples was used to estimate the missing data; this assumption is based on the consistent formation of parallel curves in all of the other tests.

The design of this experimental study permitted the evaluation of the data for statistical significance. Figure 10 is a graphical depiction of the variation and effects of the factors; A-C show effective thermal diffusivity results and D-F show effective thermal inertia results.

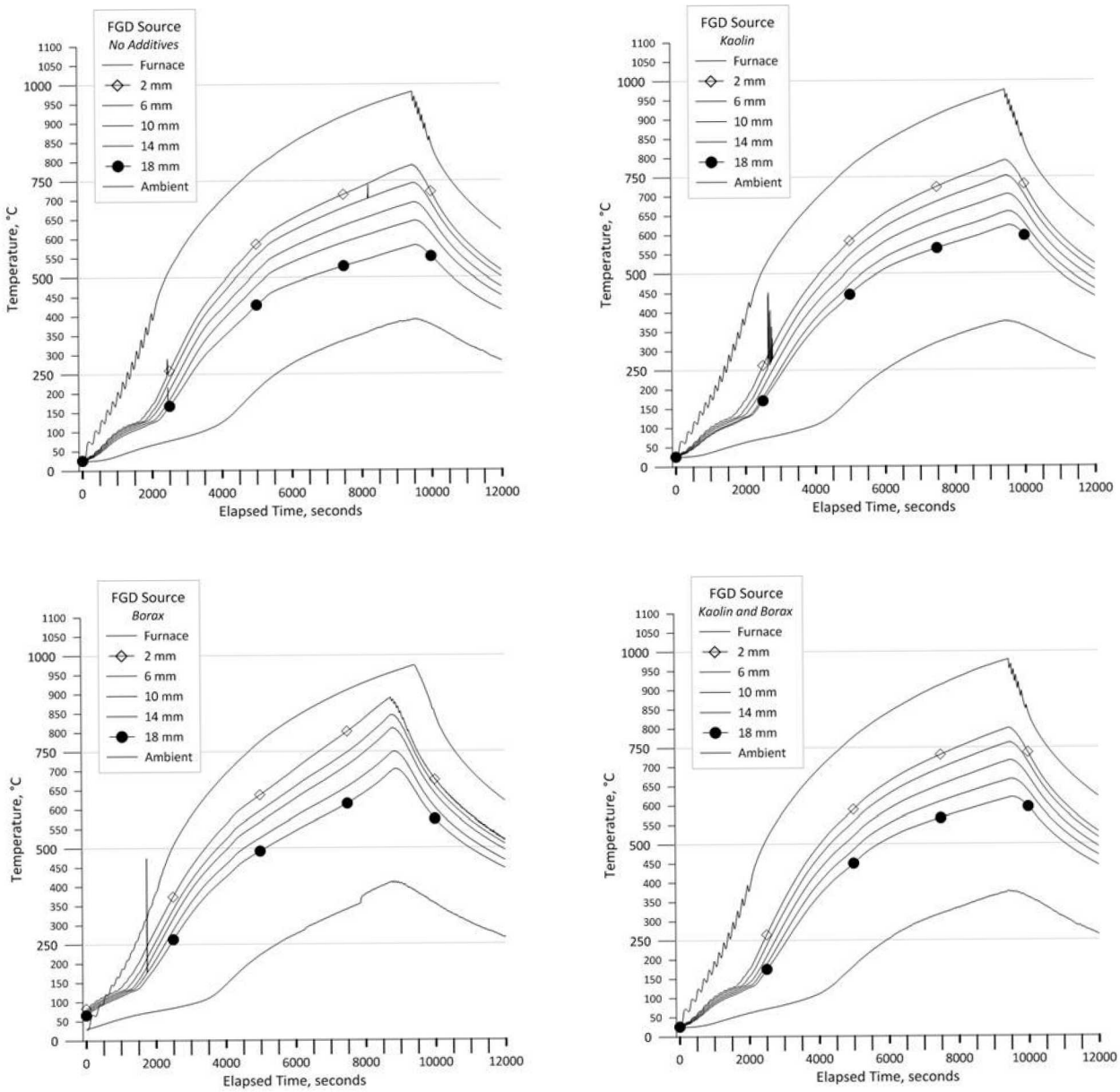


Figure 8: FGD Source - Embedded thermocouple temperatures; legend shows order of thermocouples from furnace side to ambient side.

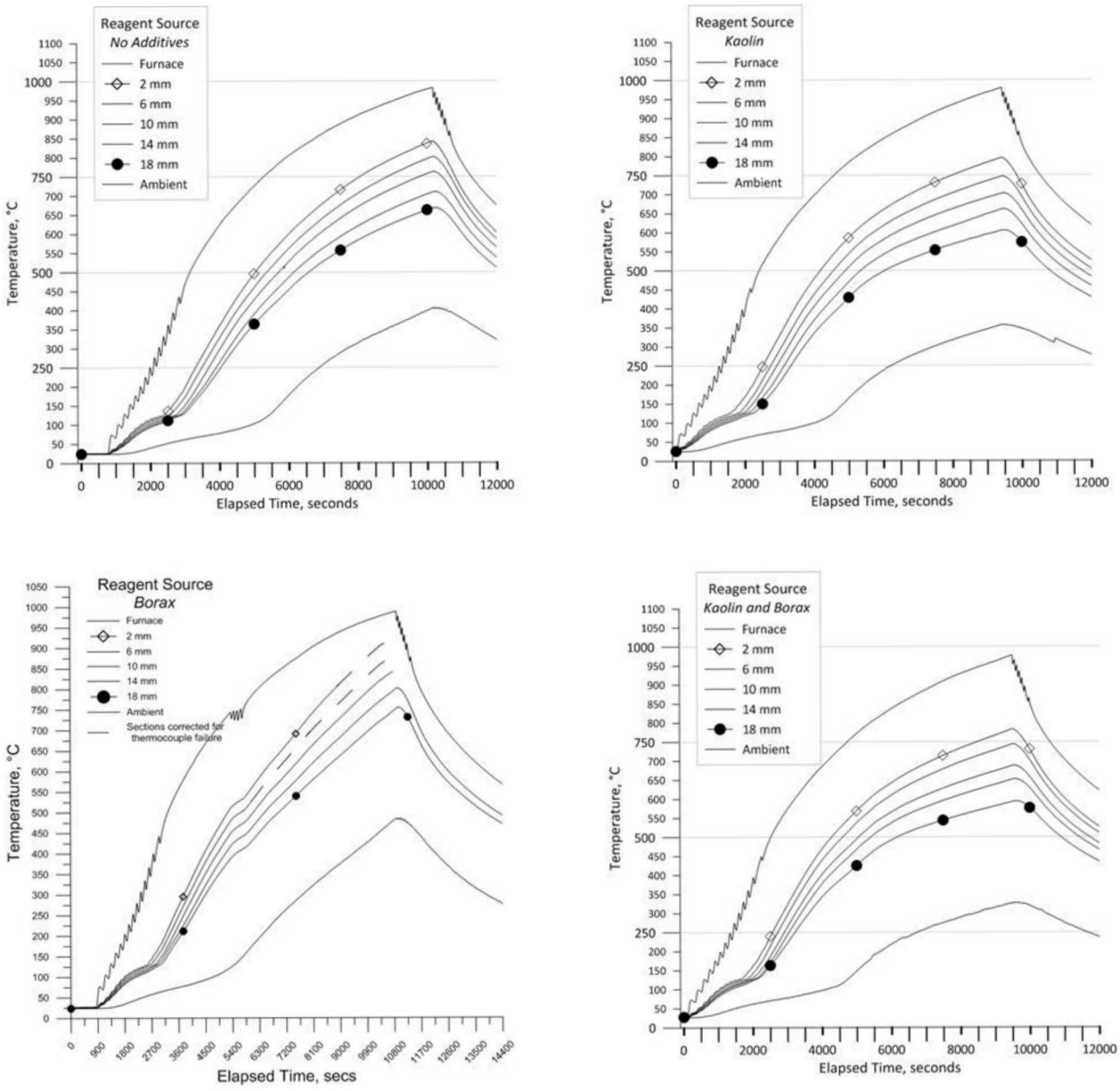


Figure 9: Reagent Source - Embedded thermocouple temperatures; legend shows order of thermocouples from furnace side to ambient side.

### 3.1 Effective thermal Diffusivity

When the original design was evaluated (Figure 10A), differences were noted in the calcination and hi-range sections. In the calcination section, the natural source has the greatest variation. In the hi-range section, the FGD has the most variation. The mid-range section had comparable values.

In the next panel (Figure 10B), the addition of kaolin was evaluated. In this series, in all cases the addition of kaolin stabilized the thermal diffusivity. And in the final panel of the diffusivity analysis (Figure 10C), borax had an effect on the thermal performance in the calcination and hi-range sections.

The analysis does not result in any of these differences being statistically significant.

### 3.2 Effective thermal Inertia

The original design (Figure 10D), which primarily evaluates the hemihydrate source, showed that FGD was different from the other two sources. The data also indicated that neither kaolin nor borax influenced the effective thermal inertia.

A Pareto analysis of the experiments (Figure 11) showed statistically significant results only for the natural:reagent comparison when borax (BC interaction) was added to the reagent source, the mid-range mean effective thermal inertia (~68 $J/(m^2 \cdot K \cdot s^{1/2})$) was reduced by ~23 $J/(m^2 \cdot K \cdot s^{1/2})$. Kaolin addition gave a non-statistically significant increase in the calcination mean effective thermal inertia (~ 30 $J/(m^2 \cdot K \cdot s^{1/2})$) of ~11 $J/(m^2 \cdot K \cdot s^{1/2})$.

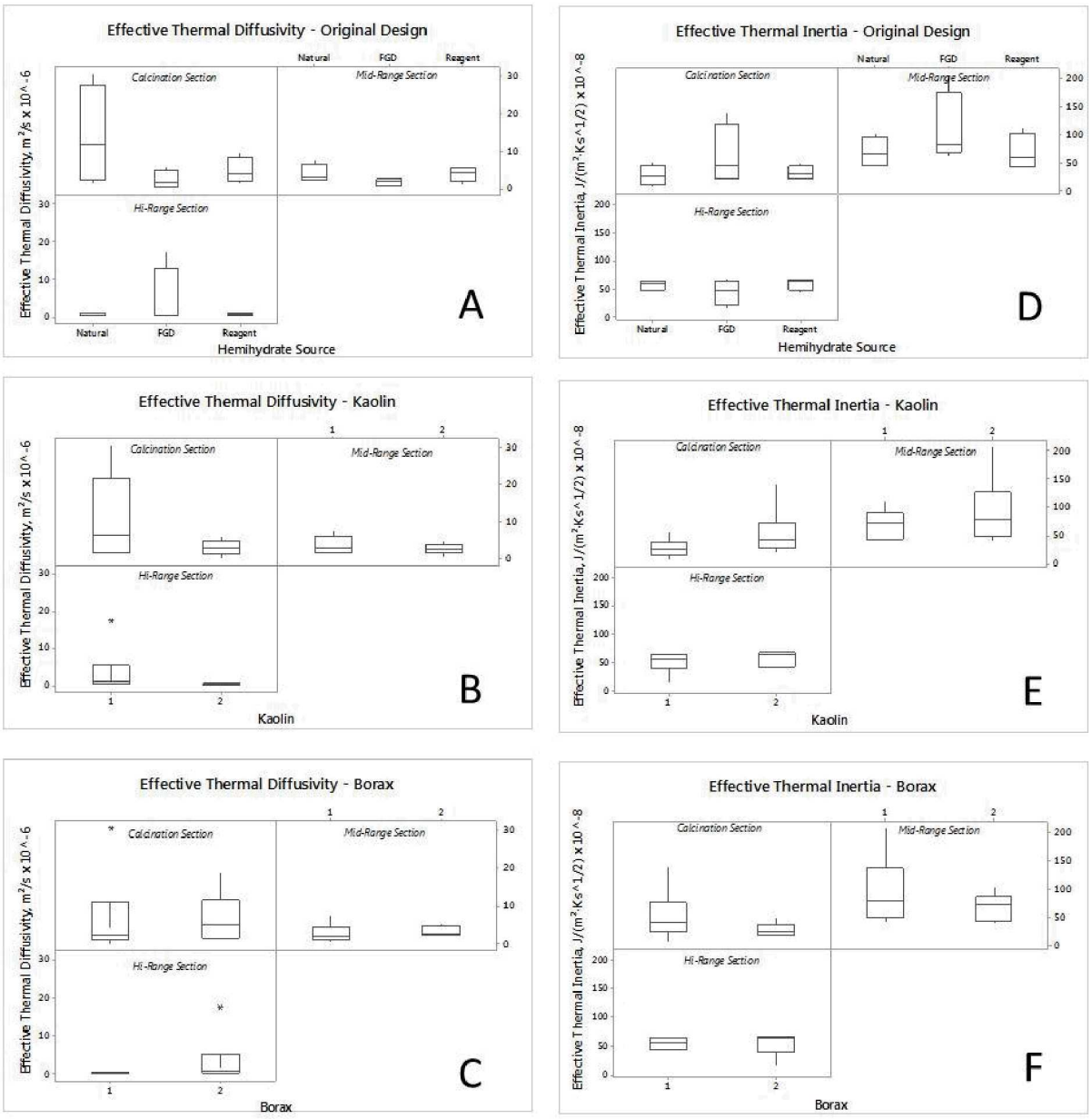


Figure 10: Summary of effective thermal diffusivity (A-C) and effective thermal inertia (D-F) by factor; in panels B, C, E, and F the value "1" indicates 'not present' and "2" indicates loading as stated in experimental design. Each image in the "box plot" graph represents an outlier with an *and from top to bottom; maximum, third quartile, median, first quartile, minimum (Help section of Minitab® 17.3.1)

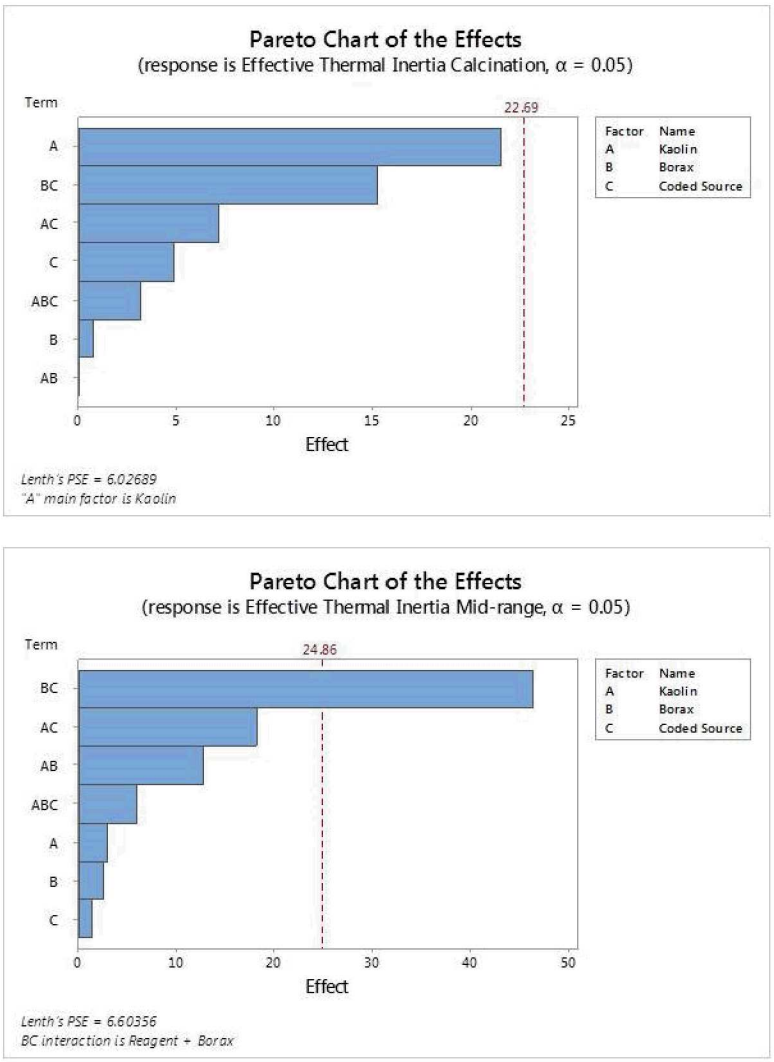


Figure 11: Pareto Analysis of significant Effective thermal Inertia results in the Natural:Reagent source comparison; upper panel is during the calcination section and the lower panel is during the mid-range section.

## 4. Conclusions

The analyses show that the thermocouple data obtained can be used to estimate *effective thermal diffusivity* and *effective thermal inertia*. These measures are affected by the hemihydrate source, by extension the impurities, and the additive. Although the factor effects are not statistically significant, the results follow the expected trend for the impurity. Even though the differences seem minor, the ASTM E119 test [3] is a timed test and changes even in fractions of a minute result in the difference between success or failure of the acceptance criteria.

Minor changes were shown to affect the speed and how much heat must be added to force the heat through the cast, which is hypothesized to mean that heat was being forced more rapidly through the slab, which will have a deleterious effect on the ignition and flame spread properties of a material [7].

## 5. Future Work

The changes being planned with respect to panel composition, especially the "lighter weight" fire resistive panels being patented by most commercial suppliers world-wide will affect many of the properties that were believed to be "understood". The authors recommend that the following work be conducted in the future:

1. For formulators, the effects at elevated temps could be evaluated by DTA/TGA and dilatometric methods. Dilatometry is recommended as part of the analysis because changes in the softening point may not be captured by DTA/TGA or DSC.
2. The author suggests that the common formulation packages being used in commercial products, i.e., starch, foaming agents, and dispersants, be separately evaluated using primary gypsum sources compared to reagent grade castings made without covering

materials. Furthermore, to assure adequate quantities of reagent grade, it should be manufactured under laboratory conditions to produce CaSO4·2H2O. The use of this technique is not recommended if there is not a laboratory calcining method to produce the hemihydrate phase.

3. An issue with small scale comparative analysis is that heating must come from one side to replicate and ASTM E119 or ISO 834 fire test. Thus leakage of heat from a furnace where one wall is not an integral part of the furnace is a large problem to supply enough energy to maintain the prescribed heating profile.

4. The authors recommend several modifications to accommodate observed changes in the specimen as it goes through the heating profile; as the heat flux moves through the specimen, the first change is that the steam from the dehydration is forced to the ambient side heating of the specimen to 100°C in a moist environment, which could result in the steam distillation, solubilization and recrystallization of some of the materials. After the heat flux has increased the temperature of the cast, two events are observed, 1) the specimen warps and cracks begin to open through the specimen, and 2) other changes, such as the cracks begin to heal on the furnace side, that are dependent on the additives and side reactions that occur during mixing. One surprising observation was that when the cracks form on the furnace side, they do not immediately propagate through the thickness of the cast even when no fiber is used.

5. Add a second set of thermocouples on the opposite side or at right angles to evaluate the uniformity of heat transfer through the casting.

## 6. Funding

The author(s) received no financial support for the research, authorship, and/or publication of this article.

## 7. Acknowledgements

The data contained in this paper were obtained in partial fulfillment of my Ph.D. studies in Material Science at New Mexico Institute of Mining and Technology, Socorro, New Mexico

Dr. Deidre Hirschfeld, Dr. Christa Hockensmith, Dr. Nikolai Kalugin, Dr. Paul Fuierer, and Dr. Paul Shipp (USG Corporation) for their advice, guidance and involvement in this project

USG Corporation, Dr. S Veeramasuneni and Dr. D. Song for allowing me to use lab space at the Corporate Innovation Center, Libertyville, IL to prepare the samples for my dissertation.

Dr. Pin Yang (Sandia Corporation, Albuquerque, NM) for his assistance in developing a technique to analyze the thermocouple data obtained on the slabs to estimate thermal diffusivity and thermal inertia.

Dr. Paul Shipp for explaining how thermal diffusivity and thermal effusivity (inertia) are used in fire safety engineering and their applicability to my study.

Sandia National Laboratories is a multimission laboratory managed and operated by National Technology and Engineering Solutions of Sandia LLC, a wholly owned subsidiary of Honeywell International Inc. for the U.S. Department of Energy's National Nuclear Security Administration under contract DE-NA0003525. The views expressed in the article do not necessarily represent the views of the U.S. Department of Energy or the United States Government. This document has been reviewed and approved for unclassified, unlimited release under SAND2018-xxxx A.

## 8. References


1. Kuntze, R.A., *Gypsum: Connecting Science and Technology*. ASTM MNL 67. 2009, ASTM International: ASTM International.
2. *ASTM C1396/C1396M Standard Specification for Gypsum Board*. ASTM International: West Conshohocken, PA.
3. *ASTM E119 Standard Test Methods for Fire Tests of Building and Construction Materials*. ASTM International: West Conshohocken, PA.
4. Badens, E., S. Veesler, and R. Boistelle, *Crystallization of gypsum from hemihydrate in presence of additives.* Journal of Crystal Growth, 1999. **198–199, Part 1**: p. 704-709.
5. Boisvert, J.-P., et al., *Hydration of calcium sulfate hemihydrate (CaSO4·12H2O) into gypsum (CaSO4·2H2O). The influence of the sodium poly(acrylate)/surface interaction and molecular weight.* Journal of Crystal Growth, 2000. **220**(4): p. 579-591.
6. Singh, N.B. and B. Middendorf, *Calcium sulphate hemihydrate hydration leading to gypsum crystallization.* Progress in Crystal Growth and Characterization of Materials, 2007. **53**(1): p. 57-77.
7. Wickström, U., *Temperature Calculation in Fire Safety Engineering*. 2016: Springer Nature.
8. Park, S.H., et al., *Determining thermal properties of gypsum board at elevated temperatures.* Fire and Materials, 2010. **34**(5): p. 237-250.
9. Benichou, N. and M.A. Sultan, *Thermal properties of lightweight-framed construction components at elevated temperatures.* Fire and Materials, 2005. **29**(3): p. 165-179.
10. Baux, C., et al., *Enhanced gypsum panels for fire protection.* Journal of Materials in Civil Engineering, 2008. **20**(1): p. 71-77.
11. Ciudad, A., et al., *Improvement of passive fire protection in a gypsum panel by adding inorganic fillers: Experiment and theory.* Applied Thermal Engineering, 2011. **31**(17-18): p. 3971-3978.
12. Waclawska, I., *Thermal decomposition of borax.* Journal of thermal Analysis, 1995. **43**(1): p. 261-.
13. Engbrecht, D.C. and D.A. Hirschfeld, *Effects of Chemical Modification on Calcium Sulfate Castings Exposed to High Temperature*, in *ASTM STP 1588 Advances in Gypsum Technologies and Building Systems*. 2015, ASTM International. p. 27.
14. Sugahara, Y., et al., *Evidence for the Formation of Interlayer Polyacrylonitrile in Kaolinite.* Clays and Clay Minerals, 1988. **36**(4): p. 343-348.
15. Sedighi-Gilani, M., et al., *Visualizing moisture release and migration in gypsum plaster board during and beyond dehydration by neutron radiography.* International Journal of Heat and Mass Transfer, 2013. **60**: p. 284-290.
16. Shepel, S.V., K.G. Wakili, and E. Hugi, *VAPOR CONVECTION IN GYPSUM PLASTERBOARD EXPOSED TO FIRE: NUMERICAL SIMULATION AND VALIDATION.* Numerical Heat Transfer Part a-Applications, 2010. **57**(12): p. 911-935.
17. Keerthan, P. and M. Mahendran, *Numerical studies of gypsum plasterboard panels under standard fire conditions.* Fire Safety Journal, 2012. **53**: p. 105-119.
18. Wullschleger, L. and K. Ghazi Wakili, *Numerical parameter study of the thermal behaviour of a gypsum plaster board at fire temperatures.* Fire and Materials, 2008. **32**(2): p. 103-119.

19. Engbrecht, D.C., *Thermal Analysis of Calcium Sulfate Dihydrate Sources Used to Manufacture Gypsum Wallboard.* Thermochimica Acta, 2016.
20. Engbrecht, D.C., *Morphological and Synergistic Effects of Additives and Naturally Occurring Impurities on Calcium Sulfate Castings*, in *Materials Science*. 2017, New Mexico Institute of Mining and Technology: Proquest Dissertations Publishing, 10263654. p. 312.
21. Shipp, P.H., *170130 exp12 07022015 v02.xlsx [Comments on diffusivity and effusivity and reference]*, D. Engbrecht, Editor. 2017.
22. Çengel, Y.A. and A.J. Ghajar, *"Heat and Mass Transfer: Fundamentals & Applications, Fifth Edition*. 2015, New York, NY 10121: McGraw-Hill Education. 968.

# 9. Tables

Effective thermal Diffusivity and Inertia Data and Calculated Values - Natural Source

| | | | No additives | Kaolin | Borax | Kaolin and Borax |
|---|---|---|---|---|---|---|
| Calcination Section | | Coefficients: $y = c + bX + aX^2$ | | | | |
| | $mm^2/°C$ | c | 1.21E+02 | 1.17E+02 | 1.24E+02 | 1.24E+02 |
| | $mm^2/°C$ | b | -1.18E+00 | -1.20E+00 | -1.17E+00 | -1.67E+00 |
| | $mm^2/°C$ | a | 6.74E-04 | 7.92E-03 | 2.17E-03 | 2.05E-02 |
| Mid-Range Section | | | | | | |
| | $mm^2/°C$ | c | 5.57E+02 | 5.46E+02 | 5.64E+02 | 5.54E+02 |
| | $mm^2/°C$ | b | -8.05E+00 | -7.96E+00 | -8.24E+00 | -8.67E+00 |
| | $mm^2/°C$ | a | 7.68E-03 | -1.50E-02 | 2.34E-02 | -3.60E-02 |
| Hi-Range Section | | | | | | |
| | $mm^2/°C$ | c | 7.64E+02 | 7.47E+02 | 7.96E+02 | 7.59E+02 |
| | $mm^2/°C$ | b | -8.77E+00 | -9.09E+00 | -9.18E+00 | -1.18E+01 |
| | $mm^2/°C$ | a | -4.89E-02 | -6.17E-02 | -2.18E-02 | 4.95E-02 |
| Calcination Section | | Coefficients: $y = c + aX$ | | | | |
| | °C/s | c | 4.74E+01 | 3.17E+00 | -1.81E+01 | 1.67E+01 |
| | °C/s | a | 4.11E-02 | 6.86E-02 | 8.15E-02 | 6.27E-02 |
| Mid-Range Section | | | | | | |
| | °C/s | c | -5.53E+01 | 7.04E+01 | -1.23E+02 | -1.54E+02 |
| | °C/s | a | 1.17E-01 | 8.65E-02 | 1.35E-01 | 1.43E-01 |
| Hi-Range Section | | | | | | |
| | °C/s | c | 4.10E+02 | 3.70E+02 | 2.97E+02 | 3.15E+02 |
| | °C/s | a | 3.23E-02 | 3.45E-02 | 5.06E-02 | 4.28E-02 |
| | | | | | | |
| Effective thermal Diffusivity | $mm^2/s$ | | | | | |
| Calcination Section | | | 3.05E+01 | 4.33E+00 | 1.88E+01 | 1.53E+00 |
| Mid-Range Section | | | 7.65E+00 | -2.88E+00 | 2.89E+00 | -1.99E+00 |
| Hi-Range Section | | | -3.30E-01 | -2.80E-01 | -1.16E+00 | 4.33E-01 |
| | | | | | | |
| Effective thermal Diffusivity | $m^2/s \times 10^{-6}$ | | | | | |
| Calcination Section | | | 30.5 | 4.3 | 18.8 | 1.5 |
| Mid-Range Section | | | 7.6 | 2.9 | 2.9 | 2.0 |
| Hi-Range Section | | | 0.3 | 0.3 | 1.2 | 0.4 |
| | | | | | | |
| Effective thermal Inertia | $J/(m^2 \cdot K \cdot s^{1/2}) \times 10^{-8}$ | | | | | |
| Calcination Section | | | 7.4 | 33 | 18.8 | 50.8 |
| Mid-Range Section | | | 42.5 | 51 | 79.5 | 101.6 |
| Hi-Range Section | | | 56.2 | 65.3 | 46.9 | 65.1 |

Effective thermal Diffusivity and Inertia Data and Calculated Values - FGD Source

| | | | No additives | Kaolin | Borax | Kaolin and Borax |
|---|---|---|---|---|---|---|
| Calcination Section | | Coefficients: $y = c + bX + aX^2$ | | | | |
| | $mm^2/°C$ | c | 1.24E+02 | 7.49E+02 | 1.32E+02 | 1.29E+02 |
| | $mm^2/°C$ | b | -1.67E+00 | -7.54E+00 | -1.56E+00 | -1.17E+00 |
| | $mm^2/°C$ | a | 2.05E-02 | -2.21E-01 | 1.38E-02 | -4.06E-03 |
| Mid-Range Section | | | | | | |
| | $mm^2/°C$ | c | 5.54E+02 | 5.50E+02 | 5.58E+02 | 5.63E+02 |
| | $mm^2/°C$ | b | -8.67E+00 | -6.44E+00 | -8.59E+00 | -7.97E+00 |
| | $mm^2/°C$ | a | -3.60E-02 | -1.50E-01 | 1.96E-02 | -2.72E-02 |
| Hi-Range Section | | | | | | |
| | $mm^2/°C$ | c | 7.59E+02 | 1.24E+02 | 8.10E+02 | 7.70E+02 |
| | $mm^2/°C$ | b | -1.18E+01 | -5.94E-01 | -1.14E+01 | -9.30E+00 |
| | $mm^2/°C$ | a | 4.95E-02 | -2.71E-02 | -1.84E-03 | -6.77E-02 |
| Calcination Section | | Coefficients: $y = c + aX$ | | | | |
| | °C/s | c | 8.57E+00 | 4.74E+01 | 5.53E+01 | 4.59E+01 |
| | °C/s | a | 7.48E-02 | 4.44E-02 | 4.11E-02 | 4.71E-02 |
| Mid-Range Section | | | | | | |
| | °C/s | c | 2.97E+01 | -1.47E+02 | 1.18E+00 | -7.26E+01 |
| | °C/s | a | 9.71E-02 | 1.43E-01 | 1.05E-01 | 1.24E-01 |
| Hi-Range Section | | | | | | |
| | °C/s | c | 3.91E+02 | 3.94E+02 | 1.96E+02 | 3.96E+02 |
| | °C/s | a | 3.21E-02 | 3.29E-02 | 6.40E-02 | 3.39E-02 |
| | | | | | | |
| Effective thermal Diffusivity | $mm^2/s$ | | | | | |
| Calcination Section | | | 1.82E+00 | -1.00E-01 | 1.50E+00 | -5.81E+00 |
| Mid-Range Section | | | -1.35E+00 | -4.78E-01 | 2.69E+00 | -2.29E+00 |
| Hi-Range Section | | | 3.24E-01 | -6.06E-01 | -1.74E+01 | -2.50E-01 |
| | | | | | | |
| Effective thermal Diffusivity | $m^2/s \times 10^{-6}$ | | | | | |
| Calcination Section | | | 1.8 | 0.1 | 1.5 | 5.8 |
| Mid-Range Section | | | 1.4 | 0.5 | 2.7 | 2.3 |
| Hi-Range Section | | | 0.3 | 0.6 | 17.4 | 0.3 |
| | | | | | | |
| Effective thermal Inertia | $J/(m^2 \cdot K \cdot s^{1/2}) \times 10^{-8}$ | | | | | |
| Calcination Section | | | 55.4 | 140 | 33.6 | 19.6 |
| Mid-Range Section | | | 83.6 | 207 | 64.2 | 82.3 |
| Hi-Range Section | | | 56.3 | 42.2 | 15.3 | 67.8 |